Addition of Protonated Water to SO_3

Cynthia Ann Pommerening, Steven M. Bachrach, and Lee S. Sunderlin*

Department of Chemistry, Northern Illinois University, DeKalb, Illinois 60115

Received: October 21, 1998; In Final Form: December 29, 1998

The potential energy surface of protonated sulfuric acid has been studied using a flowing afterglow tandem mass spectrometer and ab initio calculations. Energy-resolved collision-induced dissociation of $H_3SO_4^+$ and $H_3O^+ \cdot SO_3$ indicates that decomposition of $H_3SO_4^+$ has a substantial barrier of 224 ± 13 kJ/mol, while $H_3O^+ \cdot SO_3$ is bound by 74 ± 15 kJ/mol. Collision-induced dissociation of $H_3SO_4^+ \cdot H_2O$ and the reaction of $H_3SO_4^+$ with H_2O show that water can catalyze the dissociation of $H_3SO_4^+$. The overall potential energy surface is remarkably similar to that for the addition of H_2O to SO_3, indicating that the additional proton does not have a major effect on the reaction. The experimental and computational results are in excellent agreement for all species where sulfur is tricoordinate. When the sulfur is tetracoordinate, very large basis sets appear to be necessary for accurate energetics.

Introduction

The addition of water to sulfur trioxide to form sulfuric acid has recently received intense experimental[1−3] and computational[4,5] study. There is now general agreement that reaction 1, the gas-phase addition of H_2O to SO_3, has a substantial barrier.

$$SO_3 + H_2O \rightleftharpoons H_2SO_4 \qquad (1)$$

This barrier can be attributed to the substantial geometry deformation during the proton migration. The water protons are 2.67 Å away from the closest oxygen of SO_3 in the $H_2O \cdot SO_3$ complex,[6] and the O−H bonds are stretched to ca. 1.25 Å in the transition state.[4,5] However, the presence of an additional water molecule allows the reaction to proceed with only a slight barrier. This reaction proceeds as shown in Scheme 1, with the additional water molecule acting as a proton-transfer catalyst in a six-center cyclic intermediate.[4]

It is difficult to determine the barrier height for reaction 1 experimentally since the energy needed to drive the reaction without a catalyst is very high. This problem can be avoided for ions because translational energy can be easily added by accelerating the molecule with an electric field. This study develops a detailed potential energy surface for the reaction of *protonated* water with SO_3 to form protonated sulfuric acid, and compares this surface to that for the neutral system. The additional proton is sufficiently far from the atoms directly involved in the reaction that it should not drastically alter the observed chemistry. Ab initio calculations are also used to clarify and confirm the reaction pathways. Since sulfuric acid and protonated sulfuric acid are isoelectronic, a quantitative comparison between experiment and theory in the ionic system is a test of the calculations in the neutral system. Experimental and theoretical work on the heat of formation of $H_3SO_4^+$ itself has been published previously.[7]

Experimental Section

The flowing afterglow tandem mass spectrometer used in these experiments consists of an ion source, a flow reactor, and a tandem mass spectrometer comprising a quadrupole mass filter, an octopole ion guide,[8] a second quadrupole mass filter, and a detector. This instrument has been described in detail previously;[9] a brief description follows.

SCHEME 1

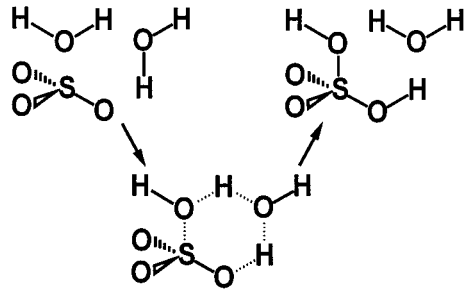

The ion source used in these experiments is a DC discharge that typically operates at 1000 V with 0.5 mA of emission current. The flow tube is a 92 cm × 7.3 cm i.d. stainless steel pipe with five neutral reagent inlets. The pressure in the flow tube is 0.4 Torr, as measured at the middle gas inlet by a capacitance manometer. The buffer gas flow velocity is 100 m/s, and approximately 10^5 collisions with the buffer gas thermalize the ions. The helium flows through a molecular sieve trap that can be cooled by liquid nitrogen to remove condensable impurities. Ions are sampled from the flow tube into the main chamber, which contains the tandem mass spectrometer. This chamber is differentially pumped to pressures sufficiently low that further collisions of the ions with the buffer gas are unlikely. The octopole passes through a gas cell that is filled with argon for collision-induced dissociation (CID) experiments or water for studies of reactive collisions.

The ions studied in this work were produced by various methods. Method A involved the addition of fuming sulfuric acid or sulfur trioxide to the ion source. Similar results were obtained by simply turning on the ionization source and desorbing sulfuric acid from the stainless steel flow tube walls.[10] When necessary, a small amount of water was added to the flow tube to improve signal intensity. This produced ions of

* Corresponding author. Telephone: 815-753-6870. Fax: 815-753-4802. E-mail: sunder@niu.edu.

10.1021/jp984104w CCC: $18.00
Published on Web 02/17/1999

m/*z* 99, which corresponds to $[H_3,S,O_4^+]$, as well as ions at masses corresponding to $[H_3,S,O_4 + (H_2O)_n]$ ($n = 1-4$). Isotope intensity patterns were consistent with these assignments. Method B involved the formation of protonated water in the ion source (from added or ambient water), followed by addition of SO_3 at a distance 40 cm downstream of the ion source. This method produced ions of the same mass as method A. The structure of the ions made by these two methods is discussed below.

Experiments with the addition of concentrated sulfuric acid gave results that varied between those of methods A and B. The concentrated acid had to be heated significantly to obtain sufficient signal intensity. Snow and Thomas observed[10] that the relative amounts of H_2SO_4, H_2O, and SO_3 in the ion source are strongly dependent on the temperature of the sulfuric acid sample, in accordance with reaction 1.

Threshold Analysis. The threshold energy for a reaction is determined by modeling the intensity of product ions as a function of the reactant ion kinetic energy in the center-of-mass (CM) frame, E_{CM}. The translational energy zero of the reactant ion beam is measured using the octopole as a retarding field analyzer.[8,11] The first derivative of the beam intensity as a function of energy is approximately Gaussian, with a full width at half-maximum of typically 1.0 eV. The laboratory energy E_{lab} is given by the octopole rod offset voltage measured with respect to the center of the Gaussian fit. Conversion to the CM frame is accomplished by use of $E_{CM} = E_{lab}m/(m + M)$, where m and M are the masses of the neutral and ionic reactants, respectively. This energy is corrected at low offset energies to account for truncation of the ion beam.[11]

Total cross sections for reaction, σ_{total}, are calculated using eq 2,[11] where I is the intensity of the reactant ion beam,

$$I = I_0 \exp(-\sigma_{total} nl) \qquad (2)$$

I_0, is the intensity of the incoming ion beam ($I_0 = I + \Sigma I_i$), and I_i are the intensities for each product ion. The number density of the neutral collision gas is n, and l is the effective collision cell length, 13 ± 2 cm.[9] Individual product cross sections σ_i are equal to $\sigma_{total}(I_i/\Sigma I_i)$.

To derive CID threshold energies, the threshold region of the data is fitted to the model function given in eq 3, where $\sigma(E)$ is the cross section for formation of the

$$\sigma(E) = \sigma_o \Sigma_i [g_i P_D(E,E_i)(E + E_i - E_T)^n/E] \qquad (3)$$

product ion at center-of-mass energy E, E_T is the desired threshold energy, σ_o is a scaling factor, n is an adjustable parameter, P_D is the probability of an ion with a given amount of energy dissociating within the experimental window (ca. 30 μs), and i denotes vibrational states having energy E_i and population g_i ($\Sigma g_i = 1$). P_D is calculated using the RRKM formalism. The CRUNCH program written by Professor P. B. Armentrout and co-workers is used in the threshold analysis described above.[11]

The data in these experiments are affected by two other sources of broadening. One is the thermal motion of the collision gas (Doppler broadening), and the other is the kinetic energy distribution of the reactant ion (which is approximated by a Gaussian function with the experimental fwhm). Both of these factors are accounted for by the CRUNCH program.

The collision gas pressure can influence the observed cross sections. An ion that is not sufficiently energized by one collision with the target gas may gain enough energy in a second collision to be above the dissociation threshold, and such collisions can lead to a measured threshold that is too low. This is accounted for by linear extrapolation of data taken at several pressures to a zero pressure cross section.[12]

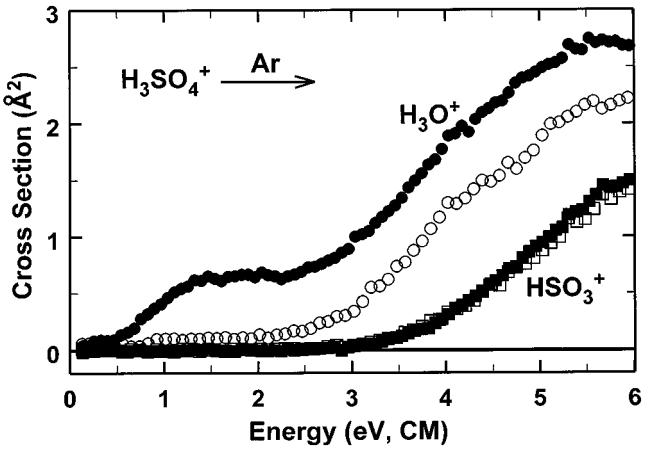

Figure 1. Appearance curves for collision-induced dissociation of $[H_3,S,O_4^+]$ as a function of kinetic energy in the center-of-mass frame. The open and closed symbols correspond to ions produced using methods A and B, respectively.

In one case the ion source was insufficiently constant to allow extrapolation of the data to the zero pressure limit. Therefore, the *thresholds* were linearly extrapolated to zero pressure. Calculated thresholds are not necessarily linearly dependent on pressure because of the effect of secondary collisions on the shape of the cross section. Consequently, extrapolation of the thresholds is not as reliable as extrapolation of the data, so the uncertainty in the derived value was doubled.

The uncertainty in the reaction thresholds due to the internal energy of the reactant ions and kinetic shifts in the thresholds was estimated by determining the threshold with the calculated frequency sets multiplied by 0.9, 1.0, and 1.1. Also, the uncertainty in the energy scale is 0.15 eV in the lab frame. These uncertainties are combined with the standard deviation of the thresholds derived from different data sets to give the overall uncertainty in reaction energetics.

Calculations. The geometries of $H_3SO_4^+$, $H_2O{\cdot}HSO_3^+$, $H_3O^+{\cdot}SO_3$, the two transition states connecting these species, and the decomposition products H_2O, H_3O^+, SO_3, and HSO_3^+, were first optimized at the HF/6-31G(d) level. Vibrational frequencies were calculated at this level for use in the internal energy and RRKM calculations. The HF zero-point vibrational energies were scaled by 0.89. The nature of the stable structures and transition states was verified by the existence of zero or one imaginary vibrational frequencies, respectively. Further optimization at the MP2/6-311+G(d,p) level was performed on these species. Density functional calculations at the B3LYP/6-311+G(d,p) level were also carried out. Intrinsic reaction path analysis confirmed that these transition states connect the correct stable molecules. All calculations were performed using Gaussian-94.[13]

Results

The cross sections for CID of $[H_3,S,O_4^+]$ with Ar are shown in Figure 1. The open and closed symbols correspond to ions produced using methods A and B, respectively. The reactions observed correspond to reactions 4 and 5, formation of water and sulfur trioxide with one of these two molecules retaining the additional proton.

$$[H_3,S,O_4^+] \rightarrow H_3O^+ + SO_3 \quad (4)$$

$$\rightarrow H_2O + HSO_3^+ \quad (5)$$

The cross sections for the reaction of $[H_3,S,O_4^+]$ produced by method A with water are shown in Figure 2. The products observed are given in reactions 6−8. Isotopic substitution was used to determine the source of the hydrogen atoms in the hydronium ion product of reaction 6; these results are discussed below.

$$[H_3,S,O_4^+] + H_2O \rightarrow H_3O^+ + [H_2,S,O_4] \quad (6)$$

$$\rightarrow 2\,H_2O + HSO_3^+ \quad (7)$$

$$\rightarrow (H_2O)_2H^+ + SO_3 \quad (8)$$

The cross section for formation of $(H_2O)_2H^+$ is independent of pressure. This indicates that the possible clustering of H_3O^+ (formed in reaction 6) with further H_2O molecules in the collision cell is negligible. At the reactant pressures used, collisional stabilization of adducts is typically very inefficient.

The cross sections for CID of $[H_2O{\cdot}H_3,S,O_4^+]$ with Ar are shown in Figure 3. The reactions observed are given in eqs 9−11. The high-energy CID spectrum of this ion and other acid−solvent clusters has been previously reported.[14] The same products as well as HSO_3^+ and HSO_2^+ were observed, and reaction 10 is dominant in both the previous and present experiments.

$$[H_2O{\bullet}H_3,S,O_4^+] \rightarrow H_3O^+ + [H_2,S,O_4] \quad (9)$$

$$\rightarrow H_2O + [H_3,S,O_4^+] \quad (10)$$

$$\rightarrow (H_2O)_2H^+ + SO_3 \quad (11)$$

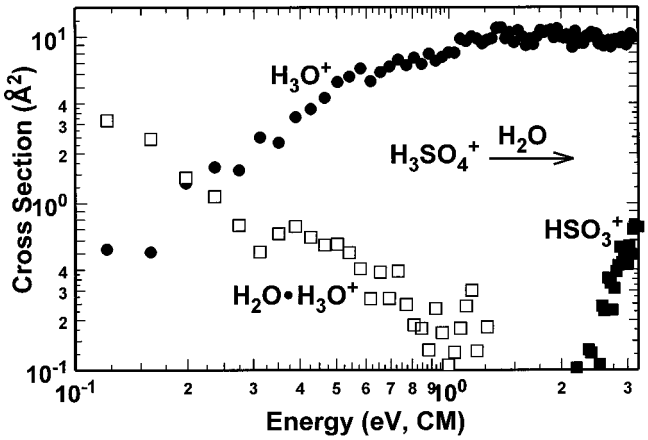

Figure 2. Appearance curves for the reaction of $H_3SO_4^+$ with H_2O as a function of kinetic energy in the center-of-mass frame.

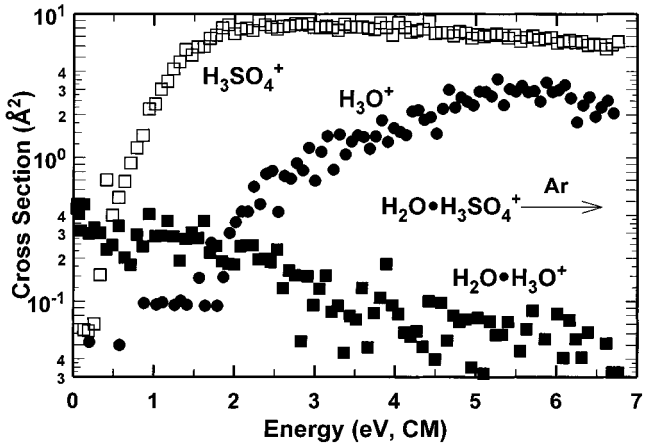

Figure 3. Appearance curves for collision-induced dissociation of $H_2O{\cdot}H_3SO_4^+$ as a function of kinetic energy in the center-of-mass frame.

Discussion

Structures for $[H_3,S,O_4^+]$. Before assigning structures to the ions seen in these experiments, the possible connectivities of $[H_3,S,O_4^+]$ need to be considered. In this discussion, it is assumed that any oxygen atom not bound to two or more hydrogen atoms is instead bound to sulfur. This rules out peroxy compounds or complexes with O_2. These structures are intuitively unreasonable. Furthermore, CID of such structures should lead to losses of fragments such as O_2, OH, or OOH, which are in fact not observed.

First, structures where the hydrogens are all attached to oxygen are considered. If all three hydrogens are attached to the same oxygen atom, the result is **I**, $H_3O^+{\cdot}SO_3$. Another possibility has two hydrogen atoms on one oxygen atom and one attached to a second oxygen atom. This gives structure **II**, HSO_3^+ solvated by water. This should be a much higher energy structure than **I** because the proton affinity of SO_3 (588 kJ/mol) is much less than that of water (691 kJ/mol).[15] Indeed, MP2/6-311+G(d,p) calculations indicate that **II** is 37 kJ/mol higher in energy than **I**. There is a small barrier to proton transfer, calculated to be 27 kJ/mol at MP2/6-311+G(d,p) and 38 kJ/mol at the B3LYP/6-311+G(d,p) level, but a barrier of this height is insufficient to prevent **II** from rearranging to **I** in the flow tube. Thus, **II** should not be a significant component of the reactant ion beam in these experiments. A third possibility is having all three hydrogen atoms attached to different oxygen atoms, which gives protonated sulfuric acid (**III**).

Structures where one or more hydrogen atoms are attached to sulfur are higher energy isomers that should not have significant barrier to proton migration, which would form the species discussed above. Thus, there are only two isomers likely to be present in the reactant ion beam: **I** and **III**.

CID of $[H_3,S,O_4^+]$. The ion populations from ion production methods A and B give CID results that are clearly different, as shown in Figure 1. Population A essentially undergoes CID only at higher energies to form both H_3O^+ and HSO_3^+; population B undergoes CID at lower energies to form H_3O^+, and has higher energy features for both products similar to those seen with population A. The fact that the type B ion population undergoes low-energy CID to form H_3O^+, while the type A population does so to only a minimal extent, indicates that one type of ion is present in significant amounts only in population B.

The possibility that **I**, the proton-bound dimer of H_2O and SO_3, only dissociates at collision energies above 2.5 eV can be ruled out because it implies an unreasonable cluster-ion bond strength for **I**. Therefore, **I** must be the isomer that dissociates at low energy and is primarily formed with type B source conditions, and the higher-energy features must be assigned to **III**. Since the cross section for formation of HSO_3^+ is the same within experimental error for both ion populations, **III** must be the predominant ion in both populations (≥90%). The drastic differences between the CID behavior of **I** and **III** allow the estimated cross sections in Figure 4 to be derived. In this figure, the maximum cross section for CID of **I** is assumed to be equal to the maximum cross section for reaction 10, dissociation of a similar proton-bound dimer. This corresponds to populations of $H_3O^+{\cdot}SO_3$ of up to roughly 10%, depending on source conditions.

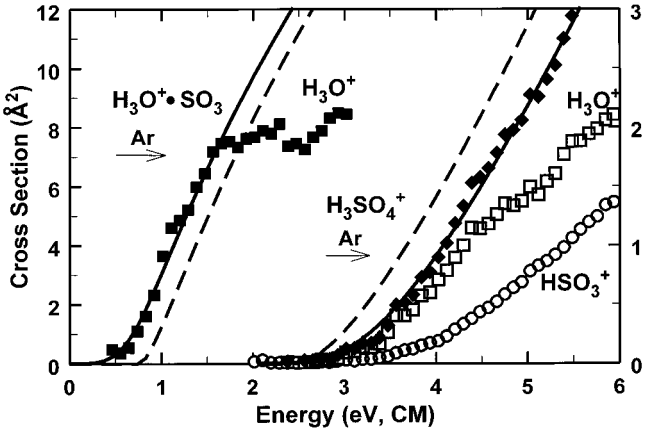

Figure 4. Appearance curves for collision-induced dissociation of $H_3SO_4^+$ and $H_3O^+ \cdot SO_3$ as a function of kinetic energy in the center-of-mass frame. The solid symbols are total cross sections, while the open symbols are individual product cross sections. The left-hand *y*-axis scale applies to CID of $H_3O^+ \cdot SO_3$, and the right-hand *y*-axis scale applies to CID of $H_3SO_4^+$. The solid lines are the model appearance curves calculated using eq 3 and convoluted as described in the text. The dashed lines are the unconvoluted fits without internal energy or kinetic shifts.

Reaction Thresholds. Three reaction onsets are shown in Figure 4. The lowest-energy onset is for reaction 12, and so corresponds to $D(H_3O^+ - SO_3)$.

$$H_3O^+ \bullet SO_3 \rightarrow H_3O^+ + SO_3 \qquad (12)$$

The kinetic shift is negligible for this reaction. The ion source for these metastable ions was insufficiently constant to allow extrapolation of the data to the zero pressure limit. Therefore, the thresholds from 10 data sets taken on five different days were linearly extrapolated to zero pressure, giving a threshold of 0.77 ± 0.07 eV. The *n* value for this fit is 1.0 ± 0.2. The uncertainty in the threshold is doubled for reasons discussed in the Experimental Section. Inclusion of the other sources of error results in a final bond energy of 74 ± 15 kJ/mol. Since SO_3 is a very weak base, it is not surprising that the binding energy of this proton-bound dimer is so low.

The other two thresholds are for CID of **III**, protonated sulfuric acid. The computational results indicate that this reaction proceeds as shown in Figure 5. First, a proton migrates from one oxygen to another oxygen that is already bound to a hydrogen atom, forming **II**. The transition state for this reaction is **IV**. **II** can then dissociate by loss of water, or rearrange by a further proton transfer to **I**. The transition states for these reactions are the $[H_2O + HSO_3^+]$ products and **V**, respectively. The weakly bound **I** can then dissociate by loss of SO_3. The computed structures of **I** to **V** are shown in Figure 6.

The measured threshold for reaction 13 must correspond to a barrier

$$H_3SO_4^+ \rightarrow H_3O^+ + SO_3 \qquad (13)$$

$$H_3SO_4^+ \rightarrow H_2O + HSO_3^+ \qquad (14)$$

in excess of the endothermicity, since the overall energy change, as calculated from known thermodynamic values in Table 1, is only 115 ± 10 kJ/mol at 0 K. The data were therefore fit using calculated frequencies for the reactant and the transition state for the first proton migration. The sum of the cross sections for reactions 13 and 14 was fit rather than the individual appearance curves because this sum represents the flux of ions passing over

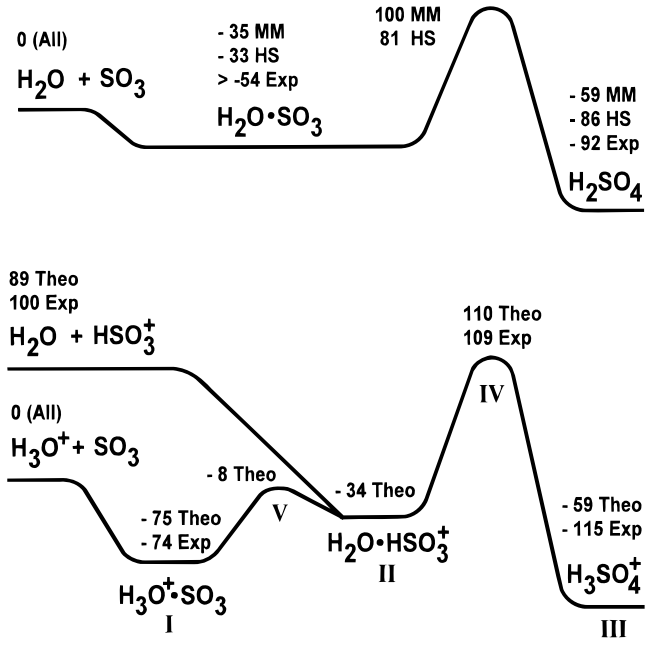

Figure 5. Experimental and computational potential energy surfaces at 0 K for the $H_3SO_4^+$ and H_2SO_4 systems. All values are referenced to the $H_2O + SO_3$ or $H_3O^+ + SO_3$ energies. The different values correspond to the following sources: MM = computational results from ref 4; HS = computational results from ref 5; Exp = results from Table 1, ref 3, and this work; Theo = computational results from this work.

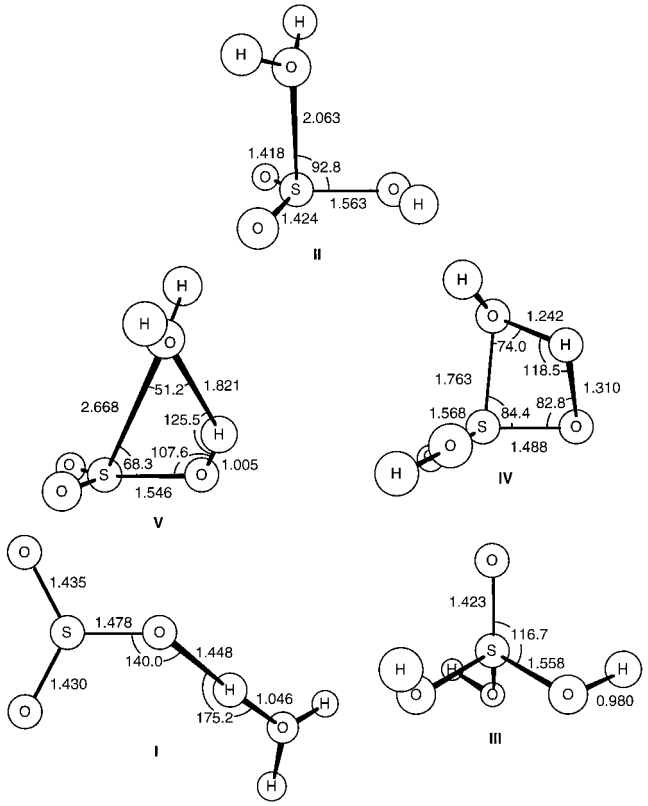

Figure 6. Structures of **I**−**V** computed at the B3LYP/6-311+G(d,p) level. Bond lengths are in Å, and bond angles are in degrees.

transition state **IV**. The calculated activation entropy is 1 ± 3 eu, which indicates the transition state is moderately tight. In a similar reaction system, the discrepancy between the measured threshold for the loss of water from $H_2PO_4^-$ and the known thermochemistry has been ascribed to a transition state tighter than the reactants.[16] The threshold for reaction 13, 2.32 ± 0.12

TABLE 1: Literature Thermochemistry

species[a]	$\Delta_f H$ (0 K)[b]	$\Delta_f H$ (298 K)	reference
H_2SO_4	-721.2 ± 8.4	-735.1 ± 8.4	15
H_2O	-238.92 ± 0.04	-241.83 ± 0.04	15
SO_3	-390.03 ± 0.71	-395.77 ± 0.71	15
H^+	1528.0 ± 0.1	1530.0 ± 0.1	15
H_3O^+	598 ± 3	597 ± 3	15
HSO_3^+	550 ± 8[c]	546 ± 8[c]	15
$H_3SO_4^+$	93 ± 9	75 ± 9	7

[a] All species in the gas phase. [b] Corrections from 298 to 0 K calculated from first principles or taken from Chase, M. W., Jr.; Davies, C. A.; Downey, J. R., Jr.; Frurip, D. J.; McDonald, R. A.; Syverud, A. N. *J. Phys. Chem. Ref. Data* **1985**, *14*, Suppl. 1. [c] Error limits estimated.

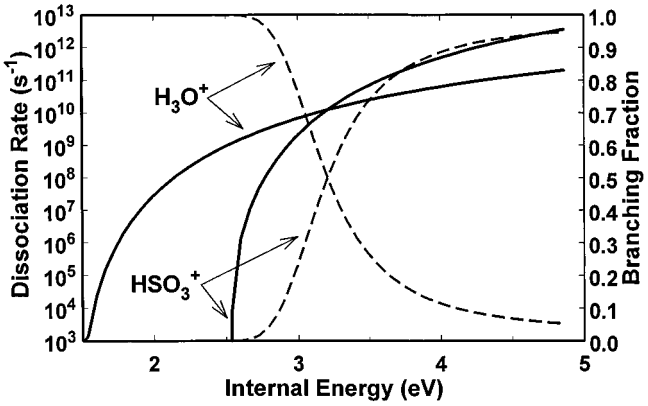

Figure 7. RRKM dissociation rates for the decomposition of $H_2O{\cdot}HSO_3^+$ as a function of internal energy (solid lines) and branching fractions for the two products (dashed lines).

eV, corresponds to a 224 ± 13 kJ/mol barrier when the other error sources are included. The *n* value used to fit this reaction is 2.0 ± 0.2.

Typical fits to the data are shown in Figure 4. This figure demonstrates the importance of accounting for the internal energy and RRKM effects. For **I**, the RRKM shift is negligible, and the convoluted fit lies to the left of the 0 K model cross section because of internal energy effects. For **III**, the RRKM shift is larger than the internal energy shift, and the order of the model cross sections is reversed.

The highest apparent threshold is for formation of HSO_3^+, reaction 14. Since the overall reaction is endothermic by 218 ± 12 kJ/mol, Table 1, the threshold for this reaction should be the same or nearly the same as for reaction 13. The explanation for the delayed onset is that there is a competitive shift for this reaction.[17] If intermediate **II** is formed with only a moderate amount of excess energy, its lifetime is sufficiently long that rearrangement by proton transfer can occur, giving reaction 13. If **II** is formed with more excess energy, it is more likely to dissociate before rearrangement. In other words, HSO_3^+ is the kinetically favored product ion while H_3O^+ is the thermodynamically favored product ion.[18]

This competition can be modeled by RRKM calculations of the relative rates of dissociation and rearrangement, using the computed parameters for the frequencies and the reaction energetics. Shown in Figure 7 are the results of this calculation using parameters at the HF/6-31G(d) level. The RRKM rates are typical for a competition between a low-energy pathway with a comparatively tight transition state and a higher-energy pathway with a looser transition state. The two rates cross at an energy of 3.2 eV. Breakdown curves showing the branching fractions of the two products as a function of internal energy are also shown in Figure 6. The breakdown curves can be summarized as follows: ions that have less than 2.6 eV of internal energy after collision with argon do not dissociate within the experimental time window, ions with between 2.6 and 3.2 eV dissociate predominantly to form H_3O^+, and ions with more than 3.2 eV of internal energy form predominantly HSO_3^+. Translational to internal energy transfer efficiencies consistent with the observed cross section shape[19] give calculated relative cross sections for the two products that agree with experiment within a factor of 2 when the HF/6-31G(d) energetics are used, but that predict substantially too much HSO_3^+ when the MP2/6-311+G(d,p) energetics are used.

Reaction of $H_3SO_4^+$ with Water. Figure 2 shows the products of the reaction of $H_3SO_4^+$ with water. The results are dramatically different from those shown in Figure 1. The H_3O^+ channel is a factor of 3 larger and has a low threshold. Because there are several reaction pathways that can lead to protonated water as a product, the reaction with D_2O was also studied. With complete scrambling, the H_3O^+:H_2DO^+:HD_2O^+ ratio should be 1:6:3. In the absence of scrambling, collisional activation of $H_3SO_4^+$ followed by delayed decomposition leads to H_3O^+, dissociation through a mechanism like that shown in Scheme 1 results in H_2DO^+, and endothermic proton transfer from $H_3SO_4^+$ to the D_2O results in HD_2O^+. Since the product ions, which may not retain much forward momentum, undergo proton exchange very efficiently with other D_2O molecules, the reaction was carried out at extremely low gas cell pressures (5 μTorr or less) to minimize further reaction.

Experimentally, H_2DO^+ is minimal at all energies (<10%), so scrambling is inefficient. The H_3O^+:HD_2O^+ ratio varies from 1:15 at low translational energies to 2:3 at three volts of reactant translational energy. This indicates that proton transfer is the dominant product at low energies, but collisional activation becomes almost as large at higher energies. Thus, the increase in the cross section for H_3O^+ is due to the proton-transfer channel, which is not observed when argon is the collision gas.

There are two other products in the reaction of $H_3SO_4^+$ with water. A small amount of HSO_3^+ is observed, apparently from CID as in the reaction with argon. A new channel is the formation of a proton-bound water dimer. The data for ion source conditions A and B are similar, so this product must be predominantly due to the $H_3SO_4^+$ isomer. This channel has a cross section that increases as translational energy approaches zero, indicating that any barrier to the reaction is negligible. This channel, then, demonstrates that water effectively catalyzes the decomposition of protonated sulfuric acid, just as in the neutral system. The decline in cross section is consistent with formation of $H_2O{\cdot}H_3SO_4^+$, followed by competition between dissociation of the proton-bound dimer and rearrangement of the acid. Once the acid has rearranged to $(H_2O)_2H^+(SO_3)$, loss of SO_3 should very rapidly give the $(H_2O)_2H^+$ product.

H_2DO^+ should be the primary product if catalytic decomposition of the acid, followed by loss of both SO_3 and water, were to occur. The lack of this product indicates that any collision complex with enough energy for two dissociations is substantially more likely to simply lose water before rearrangement. This result, as well as the small cross section for formation of $(H_2O)_2H^+$ are consistent with the expectation that the catalytic decomposition is entropically strongly disfavored.

CID of $[H_2O{\cdot}H_3,S,O_4^+]$. The data for CID of ions of mass 117 by Ar is shown in Figure 3. By far the largest cross section above 1 eV is for loss of water. If a significant fraction of the ion population were the presumably weakly bound cluster $(H_2O)_2H^+(SO_3)$, then loss of SO_3 through a loose transition state would be a major product channel at these energies. Since this

TABLE 2: Computational Results

method	$H_3O^+ + SO_3$	$H_3O^+ \cdot SO_3$	V	$H_2O \cdot HSO_3^+$	IV	$H_3SO_4^+$
HF/6-31G(d)	0	−56.4	24.6	−32.5	120.6	−117.9
MP2/6-311+G(d,p)	0	−75.1	−7.7	−34.3	110.1	−58.5
B3LYP/6-311+G(d,p)	0	−73.3	−0.7	−38.5	96.9	−72.0

is not the case, most of the ions in the beam (>99%), must be $H_2O \cdot H_3SO_4^+$ instead. Thus, the $H_3SO_4^+$ and H_3O^+ channels can be viewed as a competition for the proton in the dissociation of a proton-bound dimer. $H_3SO_4^+$, the lowest energy product, dominates at the lowest energies, but the ratio becomes more nearly even at higher energies. This behavior is typical for proton bound dimers; the kinetic method[20] uses such ratios of product intensities to determine relative affinities. Indeed, analysis of this reaction was performed previously as part of the measurement of the proton affinity of sulfuric acid.[7]

The more mechanistically interesting product is reaction 11. Although the bulk of the reactant ions are $H_2O \cdot H_3SO_4^+$, the possibility that this small product channel is due to a trace of $(H_2O)_2H^+(SO_3)$ must be considered. Collisional activation of this cluster should lead to an initial rise in the cross section for $(H_2O)_2H^+$. Furthermore, the cross section should not fall to nearly zero at high energies, since there should be a moderate chance at these energies for enough energy to be deposited for dissociation of SO_3 but not both SO_3 and H_2O. Since this is not the case, $(H_2O)_2H^+(SO_3)$ cannot be the major precursor for this product.

The dominant reactant for all products, then, must be $H_2O \cdot H_3SO_4^+$. The slowly decreasing cross section for $(H_2O)_2H^+$can be explained by noting that loss of SO_3 from this reactant must involve a rearrangement while loss of water is a simple dissociation. As with reactions 13 and 14, reaction 15 appears to be thermodynamically favored while reaction 16 is kinetically favored, and the kinetically preferred product becomes more dominant at higher energies.

$$H_2O \bullet H_3SO_4^+ \rightarrow (H_2O)_2H^+ + SO_3 \quad (15)$$

$$\rightarrow H_3SO_4^+ + H_2O \quad (16)$$

Reaction 15 confirms that water will catalyze the decomposition of protonated sulfuric acid at low energies. However, there must be at least a slight barrier to the reaction or the reactant would decompose without collisional activation. Since the proton-bound dimer $H_2O \cdot H_3SO_4^+$ starts out at a lower energy than the separated H_2O and $H_3SO_4^+$, formation of $(H_2O)_2^+$ is more uphill in energy for reaction 15 than for reaction 8 by the $H_2O-H_3SO_4^+$ binding energy, which is measured to be ~90 kJ/mol by CID.

Ion Source and Structure Comparison. The ion populations can now be correlated with the ion source conditions. A key point here is that SO_3 has a high vapor pressure at room temperature, while H_2SO_4 has a low vapor pressure. Any SO_3 added to the flow tube is rapidly converted into sulfuric acid (most probably through surface-catalyzed reactions on the flow tube walls) or pumped away.[2,21] Ions derived from sulfuric acid ($H_3SO_4^+$ or HSO_4^-) are observed weeks after the last addition of sulfuric acid or sulfur trioxide to the flow tube. Therefore, there is under essentially all conditions some amount of sulfuric acid in the flow tube. This is consistent with protonated sulfuric acid being present under all conditions in these experiments.

It seems initially odd that addition of SO_3 to the ion source produces mostly **III** and only a trace of **I**. This can be explained by noting the fate in the flow tube of three key ions: $H_3SO_4^+$, H_3O^+, and HSO_3^+. Nearly any protonated ion in the flow tube will exothermically transfer a proton to H_2SO_4 to form $H_3SO_4^+$. This appears to be a terminal ion, barring clustering reactions. The reaction of HSO_3^+ with H_2O is likely to lead to exothermic proton transfer to form H_3O^+. The reaction of H_3O^+ with SO_3 is not so exothermic, so that the complex lifetime may be long enough for collisional stabilization. This complex is initially formed with insufficient energy to rearrange to **III**. Thus, this is the only reaction likely to give product ions trapped in the metastable structure **I**. Method B, where protonated water is a major ion produced in the ion source and SO_3 is added downstream, maximizes the concentrations of the reactants for the one reaction that should lead to **I**, which explains why more **I** is seen with method B than with the other ion production methods.

Comparison of Experiment and Theory. The experimental differences in energy between different structural arrangements of $[H_3,S,O_4^+]$ and $[H_2,S,O_4]$, along with the corresponding computational energies, are shown in Figure 5. The agreement is excellent except for two species, H_2SO_4 and $H_3SO_4^+$.

Both calculations of the energetics of H_2SO_4 use large basis sets and extensive electron correlation. Morokuma and Muguruma performed the calculation at the MP4SDQ/6-311++G(d,p) level, while Hofmann and Schleyer used the MP4SDQ/6-311++G(2df,p) level. The latter level differs in having more polarization functions on the heavy atoms (2df instead of d). The larger basis set lowers the relative energy of H_2SO_4 by ca. 27 kJ/mol, bringing the result into good agreement with experiment. It also lowers the height of the transition state by 19 kJ/mol; there is no experimental value for comparison. In comparison, a 6-311++G(2d,2p) basis set was used by Bandy and Ianni for density functional studies of $H_2SO_4 \cdot nH_2O$.[22]

In the protonated system, similar results are seen. There is excellent agreement between the relative energies of the separated products, the $H_3O^+ \cdot SO_3$ cluster, and the transition state **IV**. There is a 56 kJ/mol discrepancy in the relative energy of $H_3SO_4^+$, where the MP2/6-311+G(d,p) computational results again give a higher relative energy than the experimental results. This suggests that extensive polarization functions on the heavy atoms are necessary for calculations on systems such as H_2SO_4, but are not apparently required for systems such as SO_3. Table 2 summarizes the computational results for the ionic species.

Previous experimental and computational studies at the MP4SDTQ/6-311+G(d,p)// MP2/6-31+G(d,p) level of the proton affinity of H_2SO_4 were in good agreement, giving 714 and 720 kJ/mol, respectively. Thus, any error in calculating the energy of H_2SO_4 is canceled by a similar error in the calculated energy of $H_3SO_4^+$.

As noted above, use of the higher-level energetics leads to very poor agreement between the predicted branching ratios for reactions 13 and 14, while the HF energetics give reasonable agreement. This further suggests that the MP2/6-311+G(d,p) calculation of the energy of $H_3SO_4^+$ is somewhat high, while the HF results are fortuitously more accurate.

Comparison of H_2SO_4 and $H_3SO_4^+$. As seen in Figure 5, the potential energy surfaces for protonated and nonprotonated sulfuric acid are remarkably similar. The following section compares the neutral and ion thermochemistry in more detail.

Typically, ion−neutral clusters are more strongly bound than neutral−neutral clusters because of ion−dipole and ion-induced dipole attractions. $D[H_3O^+-SO_3] = 74 \pm 15$ kJ/mol was derived above. $D[H_2O-SO_3]$ is computed to be 35 or 33 kJ/mol;[5] an experimental upper limit is 54 kJ/mol.[3]

The proton affinity of water is 691 kJ/mol, while the proton affinity of sulfuric acid is 714 kJ/mol.[7] Therefore, the endpoints of the potential energy surface for the protonated system have slightly different relative energetics than in the nonprotonated system; $H_3SO_4^+$ is lower than $H_3O^+ + SO_3$ by 115 kJ/mol at 0 K, while H_2SO_4 is lower than $H_2O + SO_3$ by a lesser amount, 92 kJ/mol. **I** is higher than **III** by 41 kJ/mol; similarly, the difference between the nonprotonated analogues is 58 kJ/mol.

The barrier for reaction −1 is calculated to be 159−167 kJ/mol.[4,5] The computational results for the protonated analogue are very similar, 169 kJ/mol. However, as discussed above, the experimental value for the protonated system is higher at 224 kJ/mol. In comparison, an apparent barrier of 140−230 kJ/mol exists for loss of water from $(HO)_2PO_2^-$.[16] This indicates that the charge on the molecule does not greatly affect the energetics of rearrangement.

The barrier for reaction −13, the addition of H_3O^+ to SO_3, equals the difference between the barrier (224 kJ/mol) and the endothermicity (115 kJ/mol) of reaction 13, or 109 ± 16 kJ/mol. The calculated MP2 value is 110 kJ/mol. The corresponding barrier to reaction 1 is calculated to be 81 kJ/mol[5] or 100 kJ/mol.[4] Thus, the barrier to addition of water is slightly higher for the HSO_3^+ system than for SO_3.

The rate of the reaction of SO_3 with water has a negative temperature dependence and a small preexponential factor.[3] These results are analogous to the negative energy dependence and low cross section observed in the present experiments. Both reactions are effectively catalyzed by water, but the transition state is entropically constrained.

Acknowledgment. We thank the American Society for Mass Spectrometry for partial support of this work through a research award to L.S.S. Acknowledgment is also made to the donors of the Petroleum Research Fund, administered by the American Chemical Society, for the partial support of this research. Peter Armentrout, Kent Ervin, and Mary Rodgers are thanked for developing the improved version of the CRUNCH data analysis program. Khanh Do and Tim Klein performed initial experiments on this system.

References and Notes

(1) Kolb, C. E.; Jayne, J. T.; Worsnop, D. R.; Molina, M. J.; Meads, R. F.; Viggiano, A. A. *J. Am. Chem. Soc.* **1994**, *116*, 10314−10315.

(2) Jayne, J. T.; Pöschl, U.; Chen, Y.-M.; Dai, D.; Molina, L. T.; Worsnop, D. R.; Kolb, C. E.; Molina, M. J. *J. Phys. Chem.* **1997**, *101*, 10000−10011.

(3) Lovejoy, E. R.; Hanson, D. R.; Huey, L. G. *J. Phys. Chem.* **1996**, *100*, 19911−19916.

(4) Morokuma, K.; Muguruma, C. *J. Am. Chem. Soc.* **1994**, *116*, 10316−10317.

(5) Hofmann, M.; Schleyer, P. von R. *J. Am. Chem. Soc.* **1994**, *116*, 4947−4952.

(6) Phillips, J. A.; Canagaratna, M.; Goodfriend, H.; Leopold, K. R. *J. Phys. Chem.* **1995**, *99*, 501−504.

(7) Do, K.; Klein, T. P.; Pommerening, C. A.; Bachrach, S. M.; Sunderlin, L. S. *J. Am. Chem. Soc.* **1998**, *120*, 6093−6096.

(8) Gerlich, D. *Adv. Chem. Phys.* **1992**, *82*, 1−176.

(9) Do, K.; Klein, T. P.; Pommerening, C. A.; Sunderlin, L. S. *J. Am. Soc. Mass Spectrom.* **1997**, *8*, 688−696.

(10) Snow, K. B.; Thomas, T. F. *Int. J. Mass Spectrom. Ion Processes* **1990**, *96*, 49−68.

(11) Ervin, K. M.; Loh, S. K.; Aristov, N.; Armentrout, P. B. *J. Phys. Chem.* **1983**, *87*, 3593. Ervin, K. M.; Armentrout, P. B. *J. Chem. Phys.* **1985**, *83*, 166−189.

(12) Loh, S. K.; Hales, D. A.; Lian, L.; Armentrout, P. B. *J. Chem. Phys.* **1989**, *90*, 5466. Schultz, R. H.; Crellin, K. C.; Armentrout, P. B. *J. Am. Chem. Soc.* **1991**, *113*, 8590.

(13) Frisch, M. J.; Trucks, G. W.; Schlegel, H. B.; Gill, P. M. W.; Johnson, B. G.; Robb, M. A.; Cheeseman, J. R.; Keith, T.; Petersson, G. A.; Montgomery, J. A.; Raghavachari, K.; Al-Laham, M. A.; Zakrzewski, V. G.; Ortiz, J. V.; Foresman, J. B.; Cioslowski, J.; Stefanov, B. B.; Nanayakkara, A.; Challacombe, M.; Peng, C. Y.; Ayala, P. Y.; Chen, W.; Wong, M. W.; Andres, J. L.; Replogle, E. S.; Gomperts, R.; Martin, R. L.; Fox, D. L.; Binkley, J. S.; Defrees, D. J.; Baker, J.; Stewart, J. J. P.; Head-Gordon, M.; Gonzales, C.; Pople, J. A. *Gaussian-94*; Gaussian, Inc.: Pittsburgh, PA, 1995.

(14) Isa, K.; Watanabe, K.; Kataoka, H.; Hirai, K.; Nakata, R. *J. Mass Spectrom. Soc. Jpn.* **1996**, *44*, 197−209.

(15) Hunter, E. P. L.; Lias, S. G. *J. Phys. Chem. Ref. Data* **1998**, *27*, 413. NIST Standard Reference Database #69, March 1998 release, Mallard, W. G., Linstrom, P. J., Eds. (http://webbook.nist.gov)

(16) Blades, A. T.; Ho, Y.; Kebarle, P. *J. Am. Chem. Soc.* **1996**, *118*, 196−201, and references therein.

(17) Lifshitz, C.; Long, F. A. *J. Chem. Phys.* **1964**, *41*, 2468−2471.

(18) McLafferty F. W.; Tureček, F. *Interpretation of Mass Spectra*, 4th ed.; University Science Books: Sausalito, CA, 1993.

(19) Rodgers, M. T.; Ervin, K. M.; Armentrout, P. B. *J. Chem Phys*. **1997**, *106*, 4499−4508. Rodgers, M. T.; Armentrout, P. B. *J. Chem. Phys.* **1998**, *109*, 1787−1800.

(20) Cooks, R. G.; Patrick, J. S.; Kotiaho, T.; McLuckey, S. A. *Mass Spectrom. Rev.* **1994**, *13*, 287−339.

(21) Wang, X.; Jin, Y. G.; Suto, M.; Lee, L. C.; O'Neal, H. E. *J. Chem. Phys.* **1988**, *89*, 4853−4860.

(22) Bandy, A. R.; Ianni, J. C. *J. Phys. Chem. A* **1998**, *102*, 6533−6539.